ACS NANO

www.acsnano.org

ARTICLE

Linker-Mediated Self-Assembly Dynamics of Charged Nanoparticles

Guanhua Lin,[†,‡,§,∥] See Wee Chee,[†,‡,§] Sanoj Raj,[⊥] Petr Král,[*,⊥,#,▽] and Utkur Mirsaidov[*,†,‡,§,∥]

[†]Department of Physics, National University of Singapore, 117551, Singapore

[‡]Centre for Advanced 2D Materials and Graphene Research Centre, National University of Singapore, 117546, Singapore

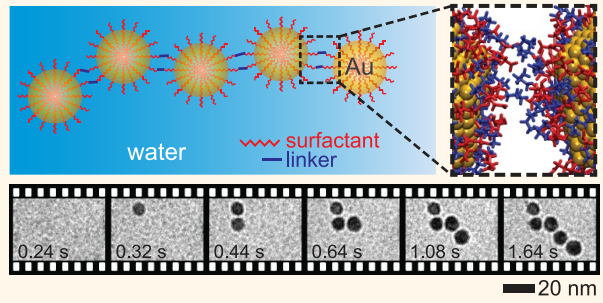
[§]Centre for BioImaging Sciences, Department of Biological Sciences, National University of Singapore, 117543, Singapore

[∥]NanoCore, National University of Singapore, 117576, Singapore

Departments of [⊥]Chemistry, [#]Physics, and [▽]Biopharmaceutical Sciences, University of Illinois at Chicago, Chicago, Illinois 60607, United States

Supporting Information

ABSTRACT: **Using *in situ* liquid cell transmission electron microscopy (TEM), we visualized a stepwise self-assembly of surfactant-coated and hydrated gold nanoparticles (NPs) into linear chains or branched networks. The NP binding is facilitated by linker molecules, ethylenediammonium, which form hydrogen bonds with surfactant molecules of neighboring NPs. The observed spacing between bound neighboring NPs, ~15 Å, matches the combined length of two surfactants and one linker molecule. Molecular dynamics simulations reveal that for lower concentrations of linkers, NPs with charged surfactants cannot be fully neutralized by strongly binding divalent linkers, so that NPs carry higher effective charges and tend to form chains, due to poor screening. The highly polar NP surfaces polarize and partly immobilize nearby water molecules, which promotes NPs binding. The presented experimental and theoretical approach allows for detail observation and explanation of self-assembly processes in colloidal nanosystems.**



KEYWORDS: *nanoparticle, self-assembly, in situ TEM, nanoparticle chains*

Self-assembly is a robust "bottom-up" fabrication method for forming nanostructures with optical,[1,2] mechanical,[3] magnetic,[4] and electrical[5] properties that are distinct from their nanoparticle (NP) building blocks and those of bulk materials.[6] The assembly of NPs into a desired structure is typically driven by interparticle interactions, external forces, or a combination of both.[7,8] Examples of NP organization directed predominantly by external forces include: assembly through evaporation of organic solvents,[9,10] assembly at liquid–liquid interfaces,[11] and DNA-directed assembly.[12] On the other hand, assembly directed solely by interparticle interactions takes advantage of intermolecular forces such as van der Waals (vdW) forces,[13,14] dipolar interactions,[15,16] $\pi-\pi$ stacking interactions,[17,18] and hydrogen bonding.[19,20] For instance, short-range hydrogen bonding is a major contributor in the assembly of NPs,[21] and organization of biological structures such as α-helices[22,23] and β-sheets.[24] The ability to understand and control these interparticle forces at the nanoscale is crucial for the formation of intricate patterns with different functionalities (*i.e.*, plasmonic assemblies for biosensing).[25]

One-dimensional (1D) NP chains are one of the simplest self-assembled structures.[26] Chains formed from gold,[27] silver,[28] or quantum dot[29] NPs have a wide range of potential applications, especially in optoelectronic,[30] biological,[31] and chemical[32] sensing. In many applications the pairwise spacing between adjacent NPs within the chain needs to be precisely defined.[33−35] This spacing between NPs in 1D structures could be controlled by introducing into the system small linker molecules that have specific interactions with NPs.[36−38] However, the sequence of steps that take place during the assembly of 1D chains with precisely spaced NPs is not yet fully understood.[39]

Herein, we studied the formation dynamics of 1D nanochains from citrate-stabilized 10 nm spherical gold NPs linked by a small molecule, ethylenediammonium, using *in situ* transmission electron microscopy (TEM) imaging in liquids.[26,40−43] The assembly dynamics in solution was visualized using TEM imaging at 25 and 100 frames per second with electron flux of 50−400 e/(Å^2·s).

Received: March 11, 2016
Accepted: August 5, 2016
Published: August 5, 2016

ACS Publications © 2016 American Chemical Society

DOI: 10.1021/acsnano.6b01721
ACS Nano 2016, 10, 7443−7450

RESULTS AND DISCUSSION

We used citrate-coated gold NPs where their binding was initiated by introduction of 50 μM ethylenediamine, into the NP suspension. Liu *et al.*[44] had previously investigated the assembly of charged gold NPs using liquid cell TEM and found that citrate stabilized gold NPs do not aggregate in water when imaged with an electron beam. This is consistent with our observations where surfactant-coated NPs remain dispersed at all times (Figure S1). However, linker molecules can promote the attachment of two adjacent NPs *via* hydrogen bonding between ethylenediammonium, protonated form of ethylenediamine in water,[45] and surfactant molecules coating the NPs as illustrated in Figure 1A. Here, two

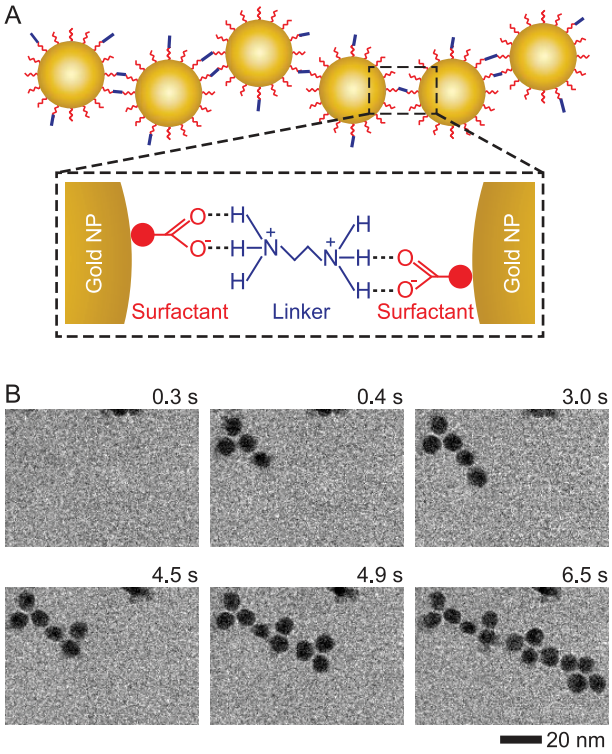


Figure 1. (A) Schematic of a gold NP chain assembly. Linker (ethylenediammonium) connects the surfactant (citrate) molecules of the adjacent gold NPs by forming hydrogen bonds between $-NH_3^+$ of ethylenediammonium and $-COO^-$ of citrate. (B) Time series of *in situ* TEM images shows the growth dynamics of a gold NP chain.

hydrogen atoms of each $-NH_3^+$ group of ethylenediammonium form hydrogen bonds with the two oxygen atoms in the $-COO^-$ group of citrate. With one $-NH_3^+$ group at each end of ethylenediammonium, up to four hydrogen bonds in total can bind two neighboring gold NPs. The net binding strength between one end of a single linker molecule and a NP is the sum of the two hydrogen bonds: N−H···O═C and N−H···O$^-$−C, which gives a binding energy of ∼12−20 k_BT (6−10 k_BT per hydrogen bond).[46] When multiple linkers bind NPs, the binding energy can be very large. This binding energy is expected to keep NPs linked together and lead to their chain formation. Figure 1B shows the sequence of images depicting assembly of the NP chain with 14 gold NPs, which is ∼100 nm in length and formed within 6.5 s.

We examined more than 150 chain formation events. Figure 2 presents various ways in which self-assembly was observed to take place. Single chains grow either by the sequential attachment of single NPs (Figure 2A) or by the addition of short chain fragments consisting of 2−3 NPs (Figure 2B). Figure 2C shows an example where the first segment already consists of three NPs. Furthermore, NPs can attach from both ends of the growing chain as seen at t = 0.84 and 2.04 s in Figure 2C. Lastly, Figure 2D shows that the existing chains can also combine into ramified structures. Here, the two growing chains labeled as *I* and *II* link up to form a branched structure. Note that these NP chains are weakly adhered to the surface and retain some degree of rotational mobility (1.12−2.52 s in Figure 2A and 0.84−1.16 s for chain *I* in Figure 2D).

To further investigate the assembly kinetics, we imaged the chain formation with a fast direct electron detection CMOS camera at a rate of 100 frames per second (Supporting Video 1). The recorded self-assembly for 10 NPs took about 1.1 s, which again reveals that the chain grows by attachment of individual NPs or short NP chain segments. It is quite clear from the movie frames in Figure 3 that even 10 ms temporal resolution is not sufficient to reveal the detailed interaction dynamics leading up to the attachment of NPs to chains.

To verify that the observed assembly dynamics of NP chains is not an artifact of the electron beam used for *in situ* TEM imaging, we compared our *in situ* results with the chains synthesized *ex situ* on the laboratory bench. NPs mixed with ethylenediamine in a test tube formed similar chains (Figure S2). Moreover, randomly dispersed gold NPs were found in both *in situ* liquid cell experiments and drop cast *ex situ* samples where ethylenediamine was absent (Figure S1). Hence, these experiments confirm that ethylenediamine is essential to linking of NPs into a chain.

Next, we examined the separation between all neighboring NPs in the chains to gain further insight into the role of linkers. Figure 4A shows the narrow distribution of the interparticle spacing between two adjacent gold NPs in 147 chains. Remarkably, the average spacing is 1.51 ± 0.11 nm, which matches well with the sum of two N−H···O hydrogen bond lengths (∼0.2 nm for each),[47] length of the linker molecule (∼0.4 nm),[48] and the combined length of two surfactant molecules (∼0.35 nm each).[49] This narrow distribution of pairwise separations (Figure 4A) further supports that the attachment between NPs is due to direct hydrogen bonding between linkers and surfactants. With a longer linker molecule, hexamethylenediamine, which has extra four $-CH_2-$ groups than ethylenediamine, the separation between the neighboring NPs increased by ∼0.5 nm (Figure S3). This difference of ∼0.5 nm is consistent with the length of extra four $-CH_2-$ groups, ∼0.52 nm,[50] and supports our hypothesis that the spacing between two adjacent NPs in the chain is controlled by the length of linkers.

Moreover, the NP ordering in a chain is highly linear (Figures 2 and 3). Figure 4B displays a histogram of the angles between three adjacent gold NPs in chains. The angle distribution is peaked at around 170°, implying the presence of a direction specific interaction between the growing chain and an incoming NP.[51,52] The aligned linear growth of the NP chains by end-to-end attachment has been suggested to be indicative of a dipolar interaction between growing chain and

DOI: 10.1021/acsnano.6b01721
ACS Nano 2016, 10, 7443−7450

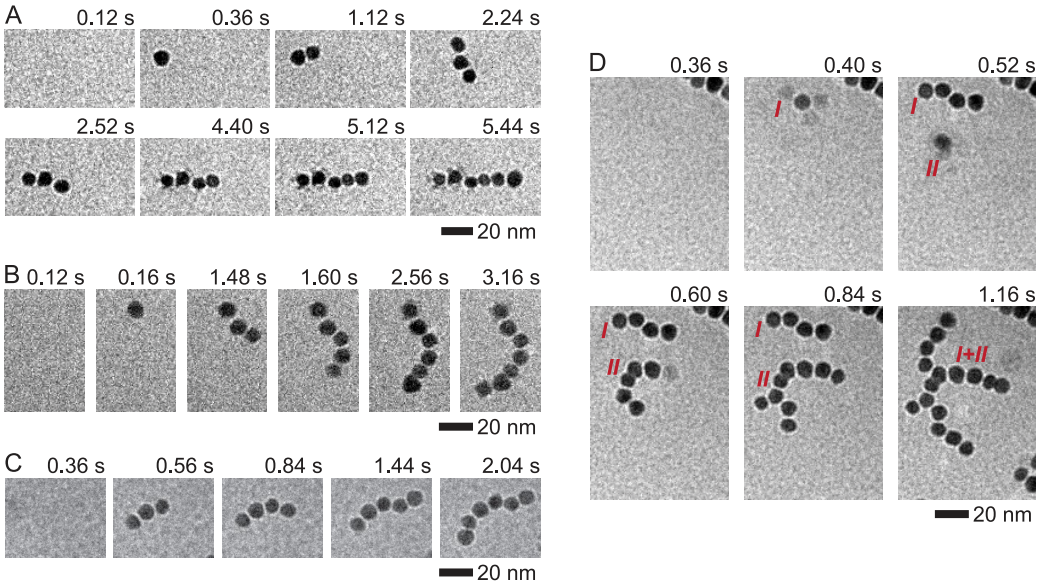


Figure 2. Time series of *in situ* TEM images of different growth modes of gold NP chains. (A) The growth of gold NP chains by assembling six monomer gold NPs together. (B, C) The growth of chains by assembling monomer, dimer, and trimer gold NPs to form the chains. (D) At t = 0.40 s, it appears that three gold NPs were attaching to form the chain *I*, subsequent images show the attachment of two chains (*I* and *II*) into a branched chain (*I* + *II*).

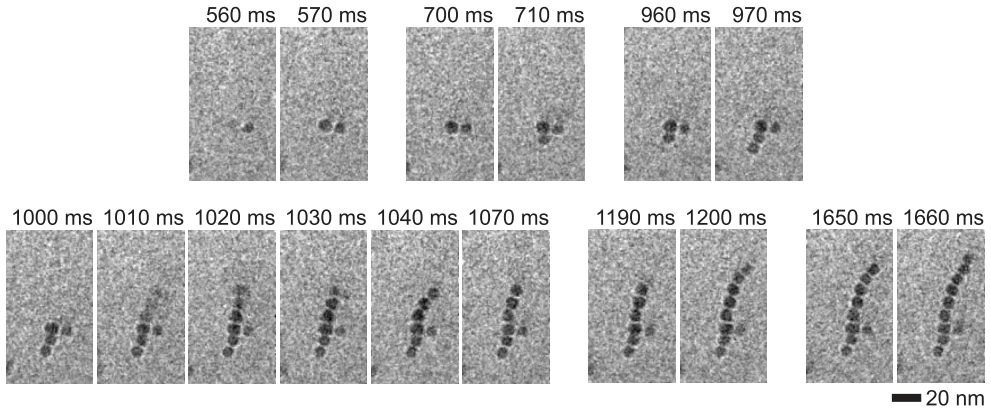


Figure 3. Time series of *in situ* TEM images showing the growth of a gold NP chain acquired at a rate of 100 frames per second (Supporting Video 1). From 560 to 970 ms, three NPs attached sequentially to form a chain. Next, at t = 1010 ms, a three-NP chain was added, after which two NPs were added at t = 1200 ms, and finally one NP was added into the chain at t = 1660 ms.

incoming NPs,[27,29,52−54] but at this point, the exact origin of dipolar interaction on chain formation is still unclear.[39]

Next, we examined how the self-assembly behavior of NPs changes with increasing concentration of added ethylenediamine linker molecules. When the concentration was increased from 50 to 250 μM, the gold NPs assembled into extensive chain networks (Figure 5A). The excess of doubly charged linkers (having a multivalent binding to the NPs) can change the NPs' charge due to the replacement of monovalent counterions with multivalent counterions. Therefore, in addition to better connectivity between NPs, linkers may also change long-range Coulombic forces between NPs during the assembly process. So it should not come as a surprise that sometimes networked structures start to form together with linear chains (Figure 2D). Figure 5B shows an image sequence describing the branched chain formation in the presence of 250 μM ethylenediamine linkers. While NPs are still added to the chain one at a time, branches extend outward from a bunched cluster of NPs (see t = 1.24 s, Figure 5B) (Supporting Video 2). Here, NPs are added at a slightly faster rate than in the case of purely linear chains (Figures 2 and 3), revealing the relative easiness with which branched NP chains form.

Atomistic molecular dynamics (MD) simulations were recently used to describe self-assembling NP systems.[55,56] To understand mechanisms controlling the self-assembly of NPs in the present study, we performed atomistic MD simulations of citrate-stabilized and hydrated gold NPs interacting through ethylenediammonium linkers at different concentrations. To match the experimental observations, we considered two cases: (i) a situation matching the self-assembly of linear chains described by a low linker concentration (Figure 6A−C), where one-half of the 702 counterion charges are provided by 175 ethylenediammonium linkers and the rest by 352 monovalent Na^+ ions, and (ii) a situation matching the self-assembly of branched chains described by a high linker concentration (Figure 6D−F), where 351 ethylenediammonium linkers are counterions. No

DOI: 10.1021/acsnano.6b01721
ACS Nano 2016, 10, 7443−7450

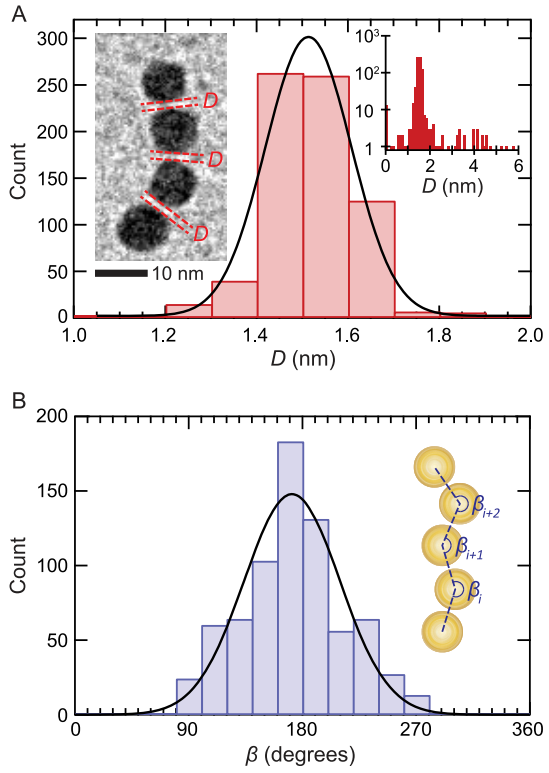


Figure 4. (A) Histogram of pairwise separations between two adjacent gold NPs in the chains displays narrow distribution of interparticle spacing centered at ~1.5 nm. Right inset shows the same distribution expanded over 6 nm range (for total of 147 chains and 919 NPs). Left inset is a TEM image of short NP chain where NP spacing, *D*, is indicated by red dashed line. (B) Histogram of angles of every three adjacent NPs in the chains. Angles are defined from one side of NP chains as shown in the inset. The attachment angle between NPs is evaluated for 150 chains and 995 gold NPs.

other ions are present in either of these systems to match the weakly screened conditions of the experiments.

We examined the possibility of NPs to form linear (Figure 6 A,D), triangular (Figure 6B,E), and L-shaped clusters (Figure 6C,F). In all the cases, two NPs are initially bound, and a third free NP is positioned at a center-to-center distance of 5–6 nm from one or both bound NPs (see Figure S5). At low linker concentration, we found that NP (3) moves away from the NP-pair (1, 2) (Figure 6A–C). This is caused by a Coulombic repulsion of the NP-pair and the free NP due to their relatively large effective equilibrium charges of about +20*e*. The linear case is the least repulsive for NP (3), but the barrier of ~40–60 k_BT can only be overcome at long time scales, which is in good agreement with the experimental results shown in Figures 2 and 3. At high linker concentration, we found that NP (3) moves closer to the NP-pair (1, 2) (Figure 6D–F) and binds in the linear configuration (Figure 6D). The NPs eventually also bind in the other geometries (Supporting Video 5). Here, the Coulombic barrier is ~25 times smaller, since the effective equilibrium charge of each NP is roughly +4*e*. This reduced barrier, due to ethylenediammonium linkers, might be too small to fit the time scales for branched chain formation observed in Figure 5, however, the overall trend of NP binding is correct.

When considering the self-assembly dynamics, besides the Coulombic interaction, we also need to consider a weak vdW attractive potential (1–3 k_BT) and very strongly distance-dependent attraction due to hydrogen bonds (Figure 6D (inset)) that form between the linkers, Na^+, and surfactants (N–H···O–C with 6–10 k_BT binding energy per bond).[46] The hydrogen bonds allow chain stabilization even in the presence of a large Coulombic repulsion (NPs (1, 2) in Figure 6A–C). Finally, we have also observed a weak attraction at large distances caused by polarized water (NP (3), and NP-pair (1, 2) in Figure 6D was attracted and coupled even when vdW coupling between the NPs in MD simulations was disconnected).

In order to clarify the origin of water-related forces, we visualized the dynamics of water molecules between NPs separated by 1 and 2 nm (Figure 7) (see Figure S6 for zoomed out view). Three water molecules were chosen in the volume between the NPs and their evolution was tracked for 300 ps. We found that during this time the selected water molecules stayed within ~1 and ~2 nm from each other for NPs separated by 1 and 2 nm, respectively. In a free-water system, individual water molecules depart ~5 nm during the same 300 ps simulation time (Figure S7). These results illustrate that water is largely immobilized between the NPs and polarized by corrugated polar NP surfaces. This localized and polarized water appears to cause additional attraction between NPs at relatively large distances, which can overcome

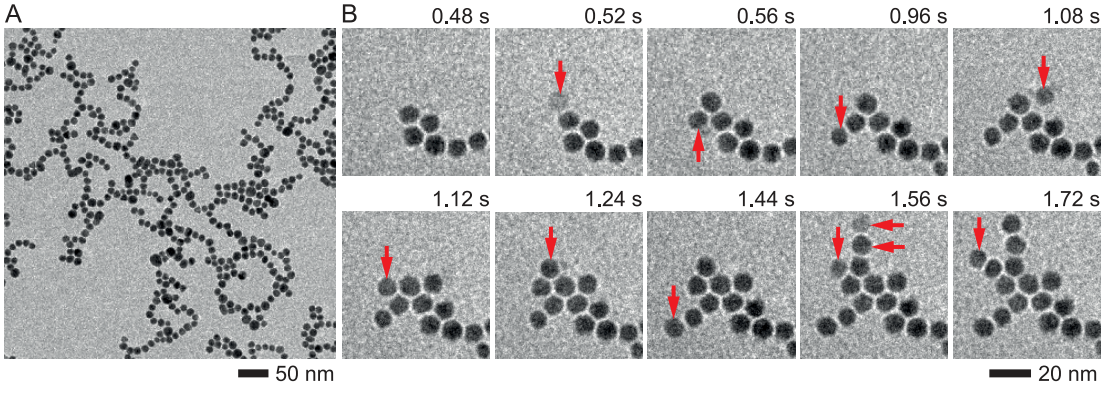


Figure 5. (A) *Ex situ* TEM image of a branched NP-chain network assembled with 250 μM ethylenediamine that has been drop-casted on a carbon film and dried. (B) *In situ* TEM image sequence showing that the formation mechanism here is the result of single NP addition. Here, the branch growth starts from a NP cluster in the presence of 250 μM ethylenediamine (Supporting Video 2).

DOI: 10.1021/acsnano.6b01721
ACS Nano 2016, 10, 7443–7450

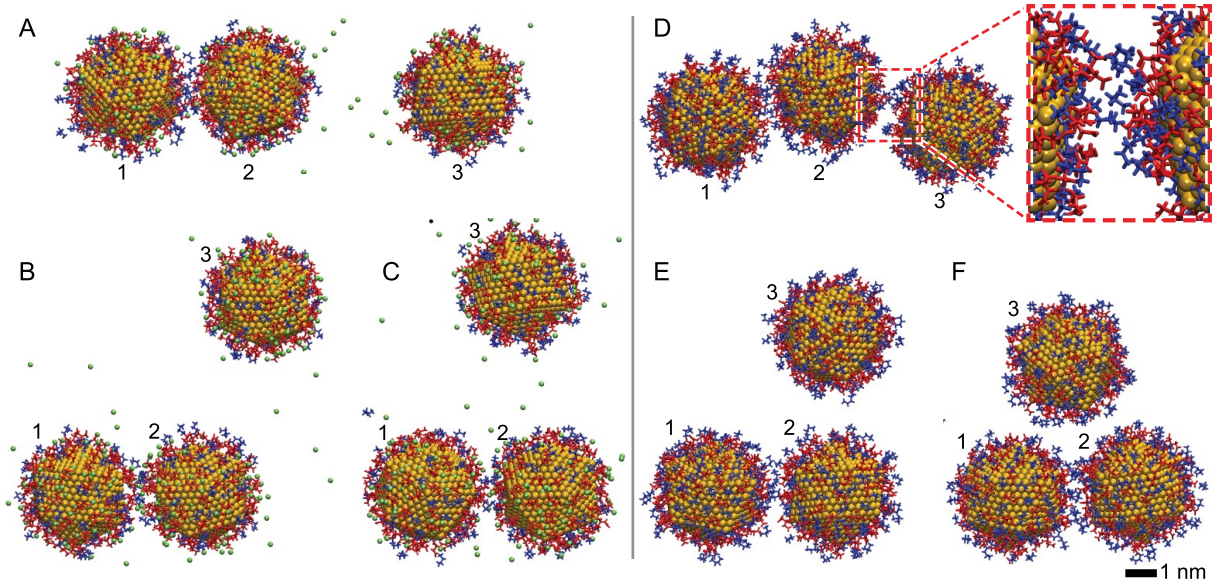


Figure 6. (A–C) Dynamics of NPs when the half of the counterions are ethylenediammonium linkers, and the other half are Na^+ ions. Motion of NP (3) away from a pair of NPs (1, 2) in 4 ns simulations, when NP (3) is initially placed (center-to-center distance): (A) 5.6 nm from NP (2) (Supporting Video 3), (B) 5.6 nm above NP (2), and (C) 5.6 nm away from both NPs (1, 2). (D–F) Only ethylenediammonium linkers are counterions. Attachment of NP (3) to a pair of NPs (1, 2) in 10 ns simulations, when NP (3) is initially placed (center-to-center distance): (D) 6.2 nm from NP (2) (Supporting Video 4); inset shows the magnified view of the attachment region, (E) 5.2 nm above NP (2) and (F) 5.2 nm away from NPs (1, 2) (Supporting Video 5). In (E, F) NP (3) stays close to linked NP-pair (1, 2) and eventually binds to them (branching). Water molecules are omitted for clarity. Orange, red, blue, and lime colors represent gold atoms, citrate molecules, ethylenediammonium linkers, and Na^+ ions, respectively. (See Figure S5 for initial configurations of NPs).

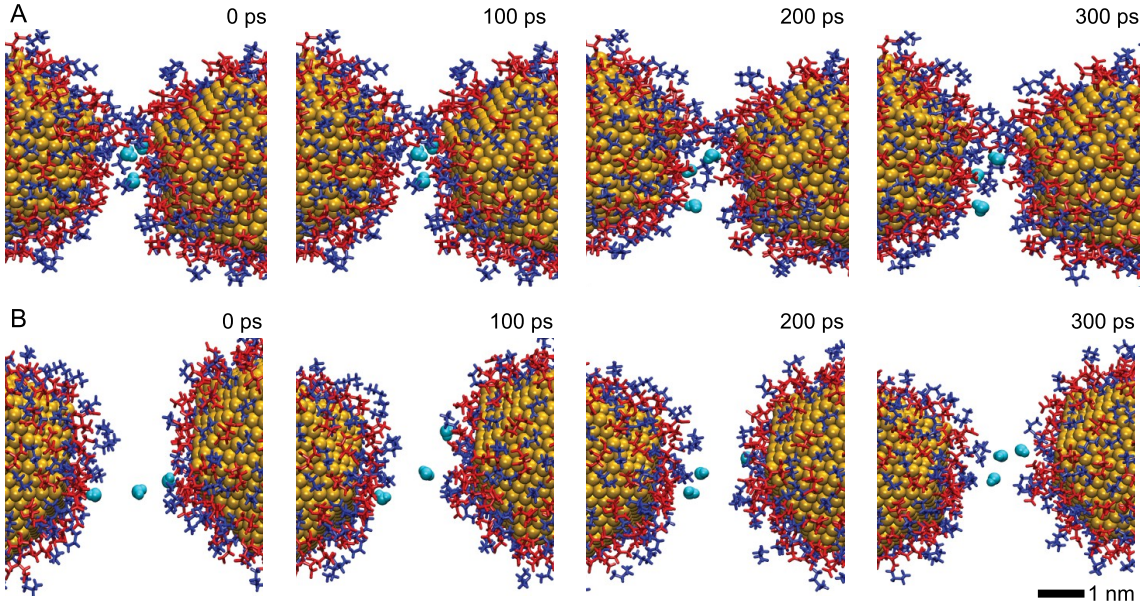


Figure 7. (A) Time dynamics of three selected water molecules (shown in cyan) between two NPs separated by ~1 nm. During 300 ps long simulations, selected water molecules stay within 1 nm from each other. (B) Time dynamics of three selected water molecules between two NPs separated by ~2 nm. Here, selected water molecules stay within 2 nm. In a free-water system, individual water molecules depart ~5 nm during the same simulation time of 300 ps.

the repulsive Coulombic barrier present between weakly charged NPs.

CONCLUSION

In conclusion, we use a combination of experimental and theoretical approaches to study the linker-mediated self-assembly dynamics of charged and polar NPs into chain-like structures with precisely defined interparticle spacing. The attachment of NPs and subsequent growth into chains is facilitated by hydrogen bonding between surfactant and linker molecules present on NPs surfaces. The combined length of surfactant and linker molecules defines the spacing between neighboring NPs. The linear and branched chain-like growth is explained by the limited availability of divalent linkers, which determine the net charge of NPs. The assembly conditions are also affected by vdW forces and correlated

DOI: 10.1021/acsnano.6b01721
ACS Nano 2016, 10, 7443–7450

forces from polarized water molecules present at NP surfaces. Further improvements in detection schemes should allow fast imaging of assembly formations, which will be important in revealing the exact nature of NP attachments.

METHODS AND MATERIALS

Sample Preparation. In our experiments, 10 nm gold NPs stabilized with citrate (cat. no. GP01-10-20, ~ 5.7×10^{12} particle/mL; Nanocs Inc., New York, NY, USA) were used as received without any further treatment. First, 300 μL of the stock gold NP solution and 5 or 25 μL of stock 10 mM ethylenediamine (cat. no. 03550-250 ML, Sigma-Aldrich Co., St Louis, MO, USA) aqueous solution were mixed with 695 μL pure water (cat. no. 320072-2.5L, Sigma-Aldrich Co., St Louis, MO, USA). Then, this solution was transferred into a syringe and slowly loaded into a liquid cell located in a Liquid Flow TEM Holder (Hummingbird Scientific, Lacey, WA, USA) *via* the connected PEEK tubing (loading speed 5 μL/min). Next, the flow holder was inserted into the TEM. Each liquid cell comprises of two flat microfabricated Si chips (2.6 × 2.6 mm) with a small SiN_x window (~200 × 30 μm) in the center.

Fabrication of Liquid Cells. The liquid cells were assembled from two flat Si chips (2.6 mm × 2.6 mm) with a small SiN_x window (~200 μm × 30 μm) in the center.[41,57] These Si chips were fabricated from 200 μm-thick double-side polished 4 in. (100) Si wafers with SiN_x film deposited on both sides by low-pressure chemical vapor deposition. The central windows and grooves separating individual chips are patterned on the SiN_x layer by photolithography, followed by deep reactive ion etching of the SiN_x layer. Next, KOH etching of the exposed Si creates the windows and the grooves. Then, the chips were cleaved from the wafer along the grooves. Finally, for each experiment, two chips were aligned based on the best overlap of the respective central windows, and a space between two membranes was sealed from the TEM column vacuum with o-rings.

Imaging. Two field emission TEMs were used for *in situ* imaging. The JEOL 2010F (JEOL Ltd., Akishima, Tokyo, Japan) was operated at an accelerating voltage of 200 kV and movies were acquired at a rate of 25 frames per second using an ORIUS SC200 CCD camera (model 830, Gatan Inc., Pleasanton, CA, USA) with the full field of view of 512 × 512 pixels (at 4 × 4 binning). For faster imaging, the liquid cells are loaded into a JEOL TEM 2200FS (JEOL Ltd., Akishima, Tokyo, Japan) operated at an accelerating voltage of 200 kV. Here movies were acquired at a rate of 100 frames per second using a direct electron detection CMOS camera (model: DE-12, Direct Electron, LP, San Diego, CA, USA) at 1024 × 1024 pixels (2 × 2 binning). The electron flux of 50–400 e/(Å^2·s) was used for all *in situ* imaging experiments. Both distance and the contact angle between NPs are measured by using ImageJ software,[58] which is an open source image processing program designed for scientific multidimensional images.

Atomistic MD Simulation. We modeled ligand-functionalized gold NPs using atomistic MD simulations. Each model NP with a gold core of 3.652 nm diameter is covered by 78 triply charged citrate ligand molecules (two charges on $-COO^-$ groups, and third charge homogeneously spread on the NP upon binding). The ligand is attached to the gold surface through the central $-COO^-$ group with a η^1-coordination.[59] The linker molecule is modeled as ethylenediammonium. CHARMM general force field[60,61] is implemented for the bond, angle, and dihedral parameters of the ligands and the linker molecules.

Nonbonding interactions were calculated using a cutoff distance of d = 10 Å, whereas long-range electrostatic interactions were calculated by the PME method[62] in the presence of periodic boundary conditions. vdW coupling of NPs was described by the potential energy acting between the NPs' gold cores:[63]

$$U(D) = -\frac{A}{6}\left(\frac{2R^2}{(4R+D)D} + \frac{2R^2}{(2R+D)^2} + \ln\frac{(4R+D)D}{(2R+D)^2}\right)$$

Here, A is the Hamaker constant for gold–gold interaction in water ($A = 3 \times 10^{-19}$ J), R = 1.826 nm is the radius of the gold core, and D is the distance between surfaces of the gold NPs. Simulations were performed with NAMD[64] in an NPT ensemble, using Langevin dynamics with a damping constant of γ_{Lang} = 0.1 ps^{-1} and a time step of 2 fs.

First, we modeled two citrate-capped gold NPs in a 170 × 140 × 140 Å^3 water box with 234 randomly distributed molecules of ethylenediammonium. Second, to form a NP pair, we placed two NPs at center-to-center separation of 52–54 Å. After 7 ns, we observed that the separation between the centers of NPs reduced to 47–48 Å at which point they are linked by linker molecules into a pair (Figure 5). Next, to model the NP chain formation, we placed a third NP on the side (linear configuration), above (triangular configuration) the linked NP-pair, or in L-shaped configuration (Figure S5) and then simulated their interaction for 10 ns.

ASSOCIATED CONTENT

Supporting Information

The Supporting Information is available free of charge on the ACS Publications website at DOI: 10.1021/acsnano.6b01721.

Supporting discussions and figures describing additional experiments and simulations (PDF)

In situ TEM movie showing formation of NP chain recorded at 100 frames per second (Video 1) (AVI)

In situ TEM movie showing formation of branched network recorded at 25 frames per second (Video 2) (AVI)

4 ns long simulation showing interaction of NPs (linear case, low linker concentration) (Video 3) (AVI)

10 ns long simulation showing interaction of NPs (linear case, high linker concentration) (Video 4) (AVI)

35 ns long simulation showing interaction of NPs (triangular case, high linker concentration) (Video 5) (AVI)

AUTHOR INFORMATION

Corresponding Authors

*E-mail: mirsaidov@nus.edu.sg.

*E-mail: pkral@uic.edu.

Notes

The authors declare no competing financial interest.

ACKNOWLEDGMENTS

This work was supported by a Young Investigator Award (NUSYIA-FY14-P17) from the National University of Singapore and the Singapore National Research Foundation's Competitive Research Program funding (NRF-CRP9-2011-04). P.K. was supported by the NSF DMR grant no. 1309765.

REFERENCES

(1) Gong, J.; Li, G.; Tang, Z. Self-assembly of noble metal nanocrystals: Fabrication, Optical Property, and Application. *Nano Today* **2012**, *7*, 564–585.

(2) Lu, Y.; Yin, Y.; Li, Z.-Y.; Xia, Y. Synthesis and Self-Assembly of Au@SiO2 Core–Shell Colloids. *Nano Lett.* **2002**, *2*, 785–788.

(3) Mueggenburg, K. E.; Lin, X.-M.; Goldsmith, R. H.; Jaeger, H. M. Elastic Membranes of Close-Packed Nanoparticle Arrays. *Nat. Mater.* **2007**, *6*, 656–660.

(4) Singh, G.; Chan, H.; Baskin, A.; Gelman, E.; Repnin, N.; Král, P.; Klajn, R. Self-Assembly of Magnetite Nanocubes into Helical Superstructures. *Science* **2014**, *345*, 1149–1153.

(5) Luther, J. M.; Law, M.; Song, Q.; Perkins, C. L.; Beard, M. C.; Nozik, A. J. Structural, Optical, and Electrical Properties of Self-

DOI: 10.1021/acsnano.6b01721
ACS Nano 2016, 10, 7443–7450

Assembled Films of PbSe Nanocrystals Treated with 1,2-Ethanedithiol. *ACS Nano* **2008**, *2*, 271−280.
(6) Brust, M.; Bethell, D.; Kiely, C. J.; Schiffrin, D. J. Self-Assembled Gold Nanoparticle Thin Films with Nonmetallic Optical and Electronic Properties. *Langmuir* **1998**, *14*, 5425−5429.
(7) Min, Y.; Akbulut, M.; Kristiansen, K.; Golan, Y.; Israelachvili, J. The Role of Interparticle and External Forces in Nanoparticle Assembly. *Nat. Mater.* **2008**, *7*, 527−538.
(8) Silvera Batista, C. A.; Larson, R. G.; Kotov, N. A. Nonadditivity of Nanoparticle Interactions. *Science* **2015**, *350*, 1242477.
(9) Xiong, Y.; Deng, K.; Jia, Y.; He, L.; Chang, L.; Zhi, L.; Tang, Z. Crucial Role of Anions on Arrangement of Cu_2S Nanocrystal Superstructures. *Small* **2014**, *10*, 1523−1528.
(10) Bigioni, T. P.; Lin, X.-M.; Nguyen, T. T.; Corwin, E. I.; Witten, T. A.; Jaeger, H. M. Kinetically Driven Self-Assembly of Highly Ordered Nanoparticle Monolayers. *Nat. Mater.* **2006**, *5*, 265−270.
(11) Lin, Y.; Skaff, H.; Emrick, T.; Dinsmore, A. D.; Russell, T. P. Nanoparticle Assembly and Transport at Liquid-Liquid Interfaces. *Science* **2003**, *299*, 226−229.
(12) Mirkin, C. A.; Letsinger, R. L.; Mucic, R. C.; Storhoff, J. J. A DNA-Based Method for Rationally Assembling Nanoparticles into Macroscopic Materials. *Nature* **1996**, *382*, 607−609.
(13) Murray, C. B.; Kagan, C. R.; Bawendi, M. G. Self-Organization of CdSe Nanocrystallites into Three-Dimensional Quantum Dot Superlattices. *Science* **1995**, *270*, 1335−1338.
(14) Gobre, V. V.; Tkatchenko, A. Scaling Laws for Van Der Waals Interactions in Nanostructured Materials. *Nat. Commun.* **2013**, *4*, 2341.
(15) Lu, C.; Tang, Z. Advanced Inorganic Nanoarchitectures from Oriented Self-Assembly. *Adv. Mater.* **2016**, *28*, 1096−1108.
(16) Talapin, D. V.; Shevchenko, E. V.; Murray, C. B.; Titov, A. V.; Král, P. Dipole−Dipole Interactions in Nanoparticle Superlattices. *Nano Lett.* **2007**, *7*, 1213−1219.
(17) Jin, J.; Iyoda, T.; Cao, C.; Song, Y.; Jiang, L.; Li, T. J.; Zhu, D. B. Self-Assembly of Uniform Spherical Aggregates of Magnetic Nanoparticles through $\pi-\pi$ Interactions. *Angew. Chem., Int. Ed.* **2001**, *40*, 2135−2138.
(18) Caputo, G.; Pinna, N. Nanoparticle Self-Assembly Using $\pi-\pi$ Interactions. *J. Mater. Chem. A* **2013**, *1*, 2370−2378.
(19) Boal, A. K.; Ilhan, F.; DeRouchey, J. E.; Thurn-Albrecht, T.; Russell, T. P.; Rotello, V. M. Self-Assembly of Nanoparticles into Structured Spherical and Network Aggregates. *Nature* **2000**, *404*, 746−748.
(20) Carroll, J. B.; Frankamp, B. L.; Rotello, V. M. Self-Assembly of Gold Nanoparticles through Tandem Hydrogen Bonding and Polyoligosilsequioxane (POSS)-POSS Recognition Processes. *Chem. Commun.* **2002**, 1892−1893.
(21) Sun, Z.; Ni, W.; Yang, Z.; Kou, X.; Li, L.; Wang, J. pH-Controlled Reversible Assembly and Disassembly of Gold Nanorods. *Small* **2008**, *4*, 1287−1292.
(22) García, A. E.; Sanbonmatsu, K. Y. α-Helical Stabilization by Side Chain Shielding of Backbone Hydrogen Bonds. *Proc. Natl. Acad. Sci. U. S. A.* **2002**, *99*, 2782−2787.
(23) Pauling, L.; Corey, R. B.; Branson, H. R. The Structure of Proteins: Two Hydrogen-Bonded Helical Configurations of the Polypeptide Chain. *Proc. Natl. Acad. Sci. U. S. A.* **1951**, *37*, 205−211.
(24) Deechongkit, S.; Nguyen, H.; Powers, E. T.; Dawson, P. E.; Gruebele, M.; Kelly, J. W. Context-Dependent Contributions of Backbone Hydrogen Bonding to β-Sheet Folding Energetics. *Nature* **2004**, *430*, 101−105.
(25) Wu, X.; Xu, L.; Liu, L.; Ma, W.; Yin, H.; Kuang, H.; Wang, L.; Xu, C.; Kotov, N. A. Unexpected Chirality of Nanoparticle Dimers and Ultrasensitive Chiroplasmonic Bioanalysis. *J. Am. Chem. Soc.* **2013**, *135*, 18629−18636.
(26) Caswell, K. K.; Wilson, J. N.; Bunz, U. H. F.; Murphy, C. J. Preferential End-to-End Assembly of Gold Nanorods by Biotin−Streptavidin Connectors. *J. Am. Chem. Soc.* **2003**, *125*, 13914−13915.
(27) Li, M.; Johnson, S.; Guo, H.; Dujardin, E.; Mann, S. A Generalized Mechanism for Ligand-Induced Dipolar Assembly of Plasmonic Gold Nanoparticle Chain Networks. *Adv. Funct. Mater.* **2011**, *21*, 851−859.
(28) Yan, C. C.; Zhang, D. H.; Li, D. D. Spherical Metallic Nanoparticle Arrays for Super-Resolution Imaging. *J. Appl. Phys.* **2011**, *109*, 063105.
(29) Tang, Z.; Kotov, N. A.; Giersig, M. Spontaneous Organization of Single CdTe Nanoparticles into Luminescent Nanowires. *Science* **2002**, *297*, 237−240.
(30) Maier, S. A.; Kik, P. G.; Atwater, H. A.; Meltzer, S.; Harel, E.; Koel, B. E.; Requicha, A. A. G. Local Detection of Electromagnetic Energy Transport below the Diffraction Limit in Metal Nanoparticle Plasmon Waveguides. *Nat. Mater.* **2003**, *2*, 229−232.
(31) Sonnichsen, C.; Reinhard, B. M.; Liphardt, J.; Alivisatos, A. P. A Molecular Ruler Based on Plasmon Coupling of Single Gold and Silver Nanoparticles. *Nat. Biotechnol.* **2005**, *23*, 741−745.
(32) Favier, F.; Walter, E. C.; Zach, M. P.; Benter, T.; Penner, R. M. Hydrogen Sensors and Switches from Electrodeposited Palladium Mesowire Arrays. *Science* **2001**, *293*, 2227−2231.
(33) Barrow, S. J.; Funston, A. M.; Gómez, D. E.; Davis, T. J.; Mulvaney, P. Surface Plasmon Resonances in Strongly Coupled Gold Nanosphere Chains from Monomer to Hexamer. *Nano Lett.* **2011**, *11*, 4180−4187.
(34) Barrow, S. J.; Rossouw, D.; Funston, A. M.; Botton, G. A.; Mulvaney, P. Mapping Bright and Dark Modes in Gold Nanoparticle Chains using Electron Energy Loss Spectroscopy. *Nano Lett.* **2014**, *14*, 3799−3808.
(35) Lamprecht, B.; Schider, G.; Lechner, R. T.; Ditlbacher, H.; Krenn, J. R.; Leitner, A.; Aussenegg, F. R. Metal Nanoparticle Gratings: Influence of Dipolar Particle Interaction on the Plasmon Resonance. *Phys. Rev. Lett.* **2000**, *84*, 4721−4724.
(36) Tan, S. F.; Wu, L.; Yang, J. K. W.; Bai, P.; Bosman, M.; Nijhuis, C. A. Quantum Plasmon Resonances Controlled by Molecular Tunnel Junctions. *Science* **2014**, *343*, 1496−1499.
(37) Zhao, Y.; Thorkelsson, K.; Mastroianni, A. J.; Schilling, T.; Luther, J. M.; Rancatore, B. J.; Matsunaga, K.; Jinnai, H.; Wu, Y.; Poulsen, D.; Frechet, J. M. J.; Paul Alivisatos, A.; Xu, T. Small-Molecule-Directed Nanoparticle Assembly towards Stimuli-Responsive Nanocomposites. *Nat. Mater.* **2009**, *8*, 979−985.
(38) Hüsken, N.; Taylor, R. W.; Zigah, D.; Taveau, J.-C.; Lambert, O.; Scherman, O. A.; Baumberg, J. J.; Kuhn, A. Electrokinetic Assembly of One-Dimensional Nanoparticle Chains with Cucurbit[7]uril Controlled Subnanometer Junctions. *Nano Lett.* **2013**, *13*, 6016−6022.
(39) Tang, Z.; Kotov, N. A. One-Dimensional Assemblies of Nanoparticles: Preparation, Properties, and Promise. *Adv. Mater.* **2005**, *17*, 951−962.
(40) Williamson, M. J.; Tromp, R. M.; Vereecken, P. M.; Hull, R.; Ross, F. M. Dynamic Microscopy of Nanoscale Cluster Growth at the Solid-Liquid Interface. *Nat. Mater.* **2003**, *2*, 532−536.
(41) Zheng, H.; Smith, R. K.; Jun, Y.-w.; Kisielowski, C.; Dahmen, U.; Alivisatos, A. P. Observation of Single Colloidal Platinum Nanocrystal Growth Trajectories. *Science* **2009**, *324*, 1309−1312.
(42) Dukes, M. J.; Jacobs, B. W.; Morgan, D. G.; Hegde, H.; Kelly, D. F. Visualizing Nanoparticle Mobility in Liquid at Atomic Resolution. *Chem. Commun.* **2013**, *49*, 3007−3009.
(43) Ross, F. M. Opportunities and Challenges in Liquid Cell Electron Microscopy. *Science* **2015**, *350*, 9886.
(44) Liu, Y.; Lin, X.-M.; Sun, Y.; Rajh, T. *In Situ* Visualization of Self-Assembly of Charged Gold Nanoparticles. *J. Am. Chem. Soc.* **2013**, *135*, 3764−3767.
(45) Kumar, N. V.; Rao, G. N. Effect of Dielectric Constant of Medium on Protonation Equilibria of Ethylenediamine. *Chem. Spec. Bioavailab.* **2011**, *23*, 170−174.
(46) Deshmukh, M. M.; Gadre, S. R. Estimation of N−H···O−C Intramolecular Hydrogen Bond Energy in Polypeptides. *J. Phys. Chem. A* **2009**, *113*, 7927−7932.

DOI: 10.1021/acsnano.6b01721
ACS Nano 2016, 10, 7443−7450

(47) Vishweshwar, P.; Nangia, A.; Lynch, V. M. Molecular Complexes of Homologous Alkanedicarboxylic Acids with Isonicotinamide: X-ray Crystal Structures, Hydrogen Bond Synthons, and Melting Point Alternation. *Cryst. Growth Des.* **2003**, *3*, 783−790.
(48) Lee, S. J.; Mhin, B. J.; Cho, S. J.; Lee, J. Y.; Kim, K. S. *Ab initio* Studies of the Conformations of Methylamine and Ethylenediamine: Interaction Forces Affecting the Structural Stability. *J. Phys. Chem.* **1994**, *98*, 1129−1134.
(49) Lee, Z.; Jeon, K.-J.; Dato, A.; Erni, R.; Richardson, T. J.; Frenklach, M.; Radmilovic, V. Direct Imaging of Soft−Hard Interfaces Enabled by Graphene. *Nano Lett.* **2009**, *9*, 3365−3369.
(50) Craven, J. R.; Hao, Z.; Booth, C. Crystallinity of Uniform Oligo(oxyethylene) Mono-n-Alkyl Ethers Studied by X-Ray Diffraction and Differential Scanning Calorimetry. *J. Chem. Soc., Faraday Trans.* **1991**, *87*, 1183−1186.
(51) Chen, Q.; Cho, H.; Manthiram, K.; Yoshida, M.; Ye, X.; Alivisatos, A. P. Interaction Potentials of Anisotropic Nanocrystals from the Trajectory Sampling of Particle Motion using in Situ Liquid Phase Transmission Electron Microscopy. *ACS Cent. Sci.* **2015**, *1*, 33−39.
(52) Liao, H.-G.; Cui, L.; Whitelam, S.; Zheng, H. Real-Time Imaging of Pt_3Fe Nanorod Growth in Solution. *Science* **2012**, *336*, 1011−1014.
(53) Gangula, A.; Chelli, J.; Bukka, S.; Poonthiyil, V.; Podila, R.; Kannan, R.; Rao, A. M. Thione-Gold Nanoparticles Interactions: Vroman-Llike Effect, Self-Assembly and Sensing. *J. Mater. Chem.* **2012**, *22*, 22866−22872.
(54) Lin, S.; Li, M.; Dujardin, E.; Girard, C.; Mann, S. One-Dimensional Plasmon Coupling by Facile Self-Assembly of Gold Nanoparticles into Branched Chain Networks. *Adv. Mater.* **2005**, *17*, 2553−2559.
(55) Bera, M. K.; Chan, H.; Moyano, D. F.; Yu, H.; Tatur, S.; Amoanu, D.; Bu, W.; Rotello, V. M.; Meron, M.; Král, P.; Lin, B.; Schlossman, M. L. Interfacial Localization and Voltage-Tunable Arrays of Charged Nanoparticles. *Nano Lett.* **2014**, *14*, 6816−6822.
(56) Yeom, J.; Yeom, B.; Chan, H.; Smith, K. W.; Dominguez-Medina, S.; Bahng; Joong, H.; Zhao, G.; Chang, W.-S.; Chang, S.-J.; Chuvilin, A.; Melnikau, D.; Rogach, A. L.; Zhang, P.; Link, S.; Král, P.; Kotov, N. A. Chiral Templating of Self-Assembling Nanostructures by Circularly Polarized Light. *Nat. Mater.* **2015**, *14*, 66−72.
(57) Liu, Q.; Leong, F. Y.; Aabdin, Z.; Anand, U.; Si Bui Quang, T.; Mirsaidov, U. Nanodroplet Depinning from Nanoparticles. *ACS Nano* **2015**, *9*, 9020−9026.
(58) Schneider, C. A.; Rasband, W. S.; Eliceiri, K. W. NIH Image to ImageJ: 25 Years of Image Analysis. *Nat. Methods* **2012**, *9*, 671−675.
(59) Park, J.-W.; Shumaker-Parry, J. S. Structural Study of Citrate Layers on Gold Nanoparticles: Role of Intermolecular Interactions in Stabilizing Nanoparticles. *J. Am. Chem. Soc.* **2014**, *136*, 1907−1921.
(60) Vanommeslaeghe, K.; Hatcher, E.; Acharya, C.; Kundu, S.; Zhong, S.; Shim, J.; Darian, E.; Guvench, O.; Lopes, P.; Vorobyov, I.; Mackerell, A. D. CHARMM General Force Field: A Force Field for Drug-Like Molecules Compatible with the CHARMM All-Atom Additive Biological Force Fields. *J. Comput. Chem.* **2010**, *31*, 671−690.
(61) Yu, W.; He, X.; Vanommeslaeghe, K.; MacKerell, A. D. Extension of the CHARMM General Force Field to Sulfonyl-Containing Compounds and Its Utility in Biomolecular Simulations. *J. Comput. Chem.* **2012**, *33*, 2451−2468.
(62) Darden, T.; York, D.; Pedersen, L. Particle Mesh Ewald: An N log(N) Method for Ewald Sums in Large Systems. *J. Chem. Phys.* **1993**, *98*, 10089−10092.
(63) Hamaker, H. C. The London—Van Der Waals Attraction between Spherical Particles. *Physica* **1937**, *4*, 1058−1072.
(64) Phillips, J. C.; Braun, R.; Wang, W.; Gumbart, J.; Tajkhorshid, E.; Villa, E.; Chipot, C.; Skeel, R. D.; Kalé, L.; Schulten, K. Scalable Molecular Dynamics with NAMD. *J. Comput. Chem.* **2005**, *26*, 1781−1802.

DOI: 10.1021/acsnano.6b01721
ACS Nano 2016, 10, 7443−7450